Cooperativity in the Interaction of Synthetic CD40L Mimetics with CD40 and Its Implication in Cell Signaling†

Sébastien Wieckowski, Nathalie Trouche, Olivier Chaloin, Gilles Guichard, Sylvie Fournel,* and Johan Hoebeke*

CNRS UPR 9021, Immunologie et Chimie Thérapeutiques, Institut de Biologie Moléculaire et Cellulaire, 15 rue René Descartes, 67084 Strasbourg, France

Received November 24, 2006; Revised Manuscript Received January 15, 2007

ABSTRACT: CD40 ligand (CD40L) and CD40 are members of the tumor necrosis factor (TNF) and TNF receptor superfamilies, respectively. Their interaction is crucial for the development of a proper immune response. Intervention on this pathway provides an important ground for new treatments targeting autoimmune diseases or helping to fight infection and cancer. We have recently reported on the structure-based design of synthetic molecules with C_3 symmetry, named mini-CD40Ls, that can effectively mimic homotrimeric soluble CD40L. Here we show that substitution of a D-prolyl residue for the glycyl within the Lys-Gly-Tyr-Tyr CD40-binding motif leads to a complete loss of cooperativity in the interaction of the mimetic with its cognate receptor as assessed by surface plasmon resonance experiments. The ability of the modified mini-CD40L to induce apoptosis on both human and murine lymphoma cells was not affected by this mutation. However, it was unable to induce the NF-κB pathway in the mouse D1 dendritic cell line, which is essential for its complete maturation, but still activated production of IL-12 p40 mRNA. These differential effects might be partly explained by the change in rigidity of the CD40 recognition element. In this study, we not only point out the consequences of the abrogation of the cooperative property in a ligand−receptor interaction on downstream cellular events but also demonstrate the usefulness of synthetic multivalent ligands in dissecting the complex mechanisms implicated in the signalosome.

CD40 ligand (CD154 molecule) is a 39 kDa type II transmembrane glycoprotein, which belongs to the TNF family (*1*). It is mainly expressed on the surface of activated T lymphocytes in a transient manner (*2*, *3*) but also exists as a soluble extracellular and biologically active homotrimeric form (*4*, *5*). Its receptor CD40, a member of the TNF receptor (TNF-R) superfamily, is expressed on the cell surface of antigen-presenting cells (APC)[1] such as dendritic cells (DC) (*6*), B cells (*7*), macrophages/monocytes, and microglia in the nervous system (*8*). CD40 is upregulated after antigen recognition. CD40−CD40L interaction plays an important role in B cell activation and proliferation, antibody isotype class switching, cytokine production, modulation of apoptosis in the germinal center, and generation of memory B cells (*9*). Moreover, ligation of CD40 by CD40L is essential in regulating the cellular immune response in which CD40 engagement on DCs leads to their maturation for activating cytotoxic T cells by increasing the level of major histocompatibility complex (MHC) and costimulatory molecule expression and by producing a high level of T cell-stimulating cytokine interleukin-12 (IL-12) (*10*).

CD40 is also expressed on non-immune cells like fibroblasts, endothelial cells, smooth muscle cells, and some epithelial cells (*11*) and induces important biological activities in synergy with interferon-γ. For instance, in atherosclerosis, inhibition of CD40 signaling on artery epithelial cells reduced the pathology and delayed the accumulation of atherosclerotic patches (*12*, *13*). Finally, CD40 is overexpressed in a broad range of cancer cells such as carcinoma, leukemia, lymphoma, and multiple myeloma in which ligation of CD40 with an agonistic monoclonal antibody (mAb) induces apoptosis (*14*−*16*). These CD40-expressing cells are, thus, like cells expressing other members of the TNF-R family (*17*), targets for cancer immunotherapies based on agonistic mAb and recombinant soluble CD40L (*18*, *19*). CD40 exerts either potent inhibition of tumor cell proliferation or sensitization to other anticancer agents by acting directly on tumor cells or by increasing the strength of the antitumor immune response via activation of dendritic cells

† This work was supported by the Centre National de la Recherche Scientifique, the Ministère de la Recherche (ACI Jeunes Chercheurs), La Ligue contre le Cancer, the Comités du Bas-Rhin et du Haut-Rhin de la Ligue contre le Cancer, and the Agence Nationale de Recherches contre le SIDA. S.W. was supported by grants from the Ministère de la Recherche and from the Fondation pour la Recherche Médicale. N.T. was supported by La Ligue contre le Cancer.

* To whom correspondence should be addressed. S.F.: telephone, (33)3 88 41 70 24; fax, (33)3 88 61 06 80; e-mail, s.fournel@ibmc.u-strasbg.fr. J.H.: telephone, (33)3 88 41 70 24; e-mail, j.hoebeke@ibmc.u-strasbg.fr.

[1] Abbreviations: CD40L, CD40 ligand (CD154); TNF, tumor necrosis factor; TRAF, tumor necrosis factor receptor-associated factor; APC, antigen-presenting cells; DC, dendritic cells; MHC, major histocompatibility complex; k_a, association rate constant; k_d, dissociation rate constant; K_D, dissociation constant; Ab, antibody; Ig, immunoglobulin; RU, response unit (resonance unit); SPR, surface plasmon resonance; GM-CSF, granulocyte macrophage colony-stimulating factor; LPS, lipopolysaccharide; NF-κB, nuclear factor κB; IκB-α, inhibitor of NF-κB alpha; IL-12, interleukin-12; RT-PCR, reverse transcription polymerase chain reaction; GAPDH, glyceraldehyde-3-phosphate dehydrogenase; MFI, mean fluorescence intensity; $\Delta\psi_m$, mitochondrial transmembrane potential; $DiOC_6(3)$, 3,3′-dihexyloxacarbocyanine iodide; RAM, rabbit anti-mouse; SE, standard error (standard deviation of the mean); Ahx, aminohexanoic acid.

10.1021/bi602434a CCC: $37.00
Published on Web 02/24/2007

(*20*, *21*). Such strategies have already been used to increase the strength of the immune response in infectious diseases (*22*, *23*) and in cancer immunotherapy (*24*) and thus reinforced the importance of developing small-molecule CD40 agonists with no side effects and high chemical and biological stability that are amenable to large-scale production.

Active forms of soluble and membrane CD40L are noncovalently bound homotrimers (*25*), which interact with three CD40 monomers forming, like the TNF−TNFR interaction (*26*), a well-ordered stoichiometrically defined 3:3 hexameric complex essential for the initiation of proper intracellular signaling. The CD40 cytoplasmic tail lacks intrinsic enzymatic activity, but interaction with its cognate ligand allows the formation of a signalosome under the plasma membrane. Subsequently, recruitment of TNF-R-associated factor (TRAFs) adaptor proteins engages downstream pathways (*27*, *28*). Activation of CD40 signaling in DCs is initiated in lipid rafts (*29*). It also induces rapid modifications in phosphorylation of protein tyrosine kinases Lyn, Fyn, and Syk that are important for the activation of B cells (*30*). In contrast, CD40L inhibits the development of aggressive histology B lymphomas and implicates Bax (*31*). Parameters influencing the activation of distinct pathways in the various cell types are not yet well understood, and this knowledge might be useful for a controlled treatment.

We have recently reported on the structure-based design of small peptide-based molecules with C_3 symmetry that can mimic CD40L homotrimers (*32*, *33*). These mini-CD40Ls interact with CD40 and reproduce the functional cellular effects of the soluble CD40L protein on both human and mouse cells. In this report, we intended to improve the biological activities of mini-CD40Ls by restricting the conformational space accessible to the CD40-binding peptide (Lys^{143}-Gly^{144}-Tyr^{145}-Tyr^{146}). Thus, one residue was modified in the sequence of the CD40-binding motif ($Gly^{144} \rightarrow$ D-Pro) to stabilize a conformation closer to that of the loop observed in the X-ray structure of native CD40L. As cooperativity is a common process for multimeric proteins (*34*−*36*), we first used surface plasmon resonance (SPR) experiments and processed the binding kinetic constants to obtain accurate data on the cooperativity of binding. The two mimetics were then used to induce apoptosis on both human and mouse lymphoma cells and to initiate some intracellular signals in the D1 mouse dendritic cell line. We will discuss the effect of the Gly → D-Pro mutation and the importance of cooperativity during the binding for the activation of downstream signaling pathways.

MATERIALS AND METHODS

CD40L Mimetic Synthesis. Synthesis of mini-CD40L **A-1** (named CD40L mimetic **1** in our previous work) was described previously (*32*). Synthesis of modified mini-CD40L **A-11** was performed in an analogous manner except that the glycyl residue in the pentapeptide was substituted with a D-prolyl residue. A detailed account of the synthesis of mini-CD40Ls will be reported elsewhere (N. Trouche et al., manuscript in preparation). For sample preparation, ligands were dissolved in milliQ 18 MΩ water at a concentration of 1 mM before further dilution to the indicated concentrations in appropriate buffer or medium.

Reagents. Recombinant soluble human CD40−mouse Ig fusion protein (rshCD40−mIg) and recombinant soluble human CD40L coupled to the mouse CD8-α extracellular domain (rshCD40L−mCD8) were purchased from Ancell Corp. (Bayport, MN). Surfactant P20 was purchased from Biacore AB (Uppsala, Sweden). The 3,3′-dihexyloxacarbocyanine iodide $DiOC_6(3)$ dye was purchased from Interchim (Montluçon, France). Lipopolysaccharide (LPS) from *Escherichia coli* (strain 0111.B4) was obtained from Sigma-Aldrich (St. Louis, MO). Fluorescein isothiocyanate (FITC)-conjugated anti-mouse CD40 (3/23 clone), FITC anti-human CD40 (5C3 clone), phycoerythrin (PE) anti-mouse CD54 (3E2 clone), PE anti-mouse CD80 (16-10A1 clone), and PE anti-mouse CD86 (GL1 clone) mAbs were purchased from Pharmingen (San Jose, CA). Anti-IκB-α rabbit antiserum and anti-actin mouse monoclonal antibody (C4) were purchased from Pharmingen. Low-endotoxin recombinant mouse granulocyte/macrophage colony-stimulating factor (rmGM-CSF) was purchased from USBiological (Swampscott, MA). Peroxidase-labeled goat anti-mouse (GAM) and goat anti-rabbit (GAR) antibodies as well as the enhanced chemiluminescence (ECL) reagent detection kit for Western immunoblotting were purchased from Amersham (Little Chalfont, Buckinghamshire, U.K.).

Surface Plasmon Resonance (SPR) Analysis. BIAcore 3000 (Biacore AB) was used to evaluate the binding of CD40L mimetics to CD40. Flow cells of a CM5 sensor chip (Research Grade, Biacore AB) were precoated with rabbit polyclonal antibodies directed against the mouse immunoglobulin (Ig) domain (RAM-Ig, Biacore AB) using amine coupling at 30 μg/mL in 10 mM acetate buffer (pH 5.5) according to the manufacturer's instructions. The chip was then flushed with 1 M ethanolamine hydrochloride (pH 8.5) (Biacore AB) and 50 mM HCl to eliminate unbound antibody. Generally, ca. 10 000 response units (RU), corresponding to 10 ng/mm^2, of RAM-Ig was immobilized. Biosensor assays were performed at 25 °C with HBS-EP buffer [10 mM HEPES (pH 7.4) containing 0.15 M NaCl, 3.4 mM EDTA, and 0.005% (v/v) surfactant P20] as the running buffer. Capture of rshCD40−mIg and of LG11-2, a mouse IgG2a mAb directed against H2B histone used as an irrelevant control (purified by protein G affinity chromatography from hybridoma supernatant), was performed on individual flow cells at a flow rate of 5 μL/min and at a concentration allowing us to achieve equivalent protein mass binding. A small amount of protein was captured, ca. 450 RU, sufficient for the detection of the binding of the CD40 ligands, and limiting the mass transport and rebinding artifacts.

CD40L mimetics and rshCD40L−mCD8 were then injected (kinetic mode) at a flow rate of 30 μL/min over the control and CD40 channels for 4 min and allowed to dissociate for an additional 3 min. The channels were regenerated for 30 s with 50 mM HCl. A 1 Hz acquisition mode was sufficient for subsequent good assessment of kinetic constants. Control sensorgrams were subtracted from the CD40 ones and analyzed with BIAevaluation version 4.1 with various models.

The simplest "Langmuir 1:1" model was first used to assess the binding kinetics of the interaction. A complete description of equations used for kinetics data determination can be found in the *Biacore AB Handbook* and is summarized

in the Supporting Information. The trivalent analyte model (*37*, *38*) was also used to evaluate the stoichiometry and to acquire some details about the mechanism of binding, in particular, the distinct rates for all binding and conformational change events, but due to the complexity of the equations and the limited integrative possibilities offered by BIAevaluation, cooperativity was assessed with the R_{eq} values from a trivalent model with freedom in the determination of the association and dissociation rate constants of the first interaction and the R_{max} value as well as all other rate constants globally processed for the sets of concentrations of the CD40 ligands.

The accuracy of the fits was measured by the χ^2 value, which evaluates the deviation of the fitted model from the experimental points. Residuals were also shown to give better insight into whether a model is accurate as the bandwidth and its shape reveal the differences between the fitted curve and the experimental data.

Cooperativity Measurement by SPR. The cooperativity is used to describe how the binding of a ligand to a multimeric receptor can enhance the binding of additional ligand to the same multimer. Given the binding of n A molecules to multimeric molecule B (eq 1)

$$B + nA \leftrightarrow B(A)_n \tag{1}$$

Y is defined as the fractionated saturation of the binding sites at equilibrium (eq 2), with the Hill number h varying from 0 to the real number of binding sites n.

$$Y = \frac{[BA]^h}{[B]^h + [BA]^h} \tag{2}$$

Considering that the variation of the concentration of analyte is nearly nil during the injection compared to the concentration of captured ligand, the sum $[B]^h + [BA]^h$ represents the total capacity of binding on multimer B. By incorporating dissociation constant K_D (see eq S1 of the Supporting Information) into eq 2, with K_D' being the apparent affinity constant, we obtain the expression (eq 3)

$$Y = \frac{[A]^h}{[A]^h + K_D'} \tag{3}$$

Equation 3 can be rearranged to eq 4.

$$\log \frac{Y}{1 - Y} = h \log[A] - h \log K_D' \tag{4}$$

A plot of $\log[Y/(1 - Y)]$ versus $\log[A]$ is called the Hill plot and represents the logarithms of the ratio of bound molecule A to free multimer B versus logarithms of the concentration of free molecule A. This plot approximates a straight line for concentrations at which the phenomenon occurs that is neither at the saturation nor at the initial phase of the sigmoid curve. Its slope at $Y = 0.5$ is called the "Hill coefficient", denoted h, and increases with the degree of cooperativity for a maximum value of the number of real binding sites (n). By homology to the SPR-calculated values, eq 4 can be converted to eq 5.

$$\log \frac{R_{eq}}{R_{max} - R_{eq}} = h \log C - h \log K_D' \tag{5}$$

From these expressions, one can trace the plot $\log[R_{eq}/(R_{max} - R_{eq})]$ versus $\log C$, with R_{max} assessed for one set of concentrations, R_{eq} determined for individual concentrations from eq 5 with k_{a1} and k_{d1} in place of k_a and k_d, respectively, assuming that the only interaction resulting in a response (increase in mass) is the first binding to the receptor, and C as the concentration of mini-CD40L injected.

Culture of Lymphoma Cells and Measurement of Apoptosis. BL41 Burkitt lymphoma and Jurkat human T leukemia cells were cultured in RPMI 1640 (Cambrex Bioscience, Verviers, Belgium) supplemented with 10% heat-decomplemented fetal bovine serum (FBS; Dominique Dutscher, Brumath, France) and gentamicin (10 μg/mL, Cambrex). The A20 mouse lymphoma cells were cultured in RPMI supplemented with 10% heat-decomplemented FBS, gentamicin (10 μg/mL), 2 mM HEPES, and 10 μM β-mercaptoethanol. For apoptosis assays, cells (5×10^5 cells/mL) were incubated at 37 °C in flat-bottom 96-well plates in the presence of various CD40 ligands at the indicated times and concentrations in 200 μL of the respective complete medium. After incubation, cells were washed with phosphate-buffered saline (PBS) and apoptosis was evaluated by measurement of the decrease in mitochondrial transmembrane potential ($\Delta\psi_m$) associated with a reduction of the level of cationic dye $DiOC_6(3)$ uptake as detected by flow cytometry (*39*); cells were resuspended in 300 μL of PBS containing 20 nM $DiOC_6(3)$, incubated at 37 °C for 20 min, and then directly analyzed by flow cytometry.

Results are expressed as the percentage of specific apoptosis according to the following formula: % of specific apoptosis = 100(% apoptotic treated cells − % spontaneous apoptotic control cells)/(100 − % spontaneous apoptotic control cells).

Culture and Maturation of D1 Mouse Dendritic Cells. D1 cells have been described as a MHC class II-positive growth factor-dependent immature dendritic cells, derived from adult mouse spleen maintained in lineage without being transformed (*40*). Cells were cultured in nontreated plastic dishes in IMDM with HEPES and L-glutamine (Cambrex), supplemented with 10% heat-decomplemented FBS, gentamicin (10 μg/mL), 10 μM β-mercaptoethanol, and 10 ng/mL rmGM-CSF. For cellular assays, 2×10^5 cells/mL were cultured for 24 h in 24-well untreated polystyrene microplates (Evergreen Scientific, Los Angeles, CA). Then, fresh medium containing the various inducers was added. After incubation for a further 24 h, cells were washed with cold PBS and harvested with 2 mL of PBS containing 2 mM EDTA. After centrifugation, cells were resuspended in cold PBS and analyzed for cell surface phenotyping by flow cytometry or used for immunoblotting and RT-PCR.

Flow Cytometry Analysis. For measurement of apoptosis, lymphoma cells were analyzed directly after the staining procedure. For phenotyping, D1 cells were stained in PBS containing 2% FBS at 4 °C for 20 min with the various antibodies used at a concentration recommended by the manufacturer. After two washes in PBS, cells were analyzed by flow cytometry with a FACSCalibur. At least 10 000 events were acquired for each experiment using CellQuest

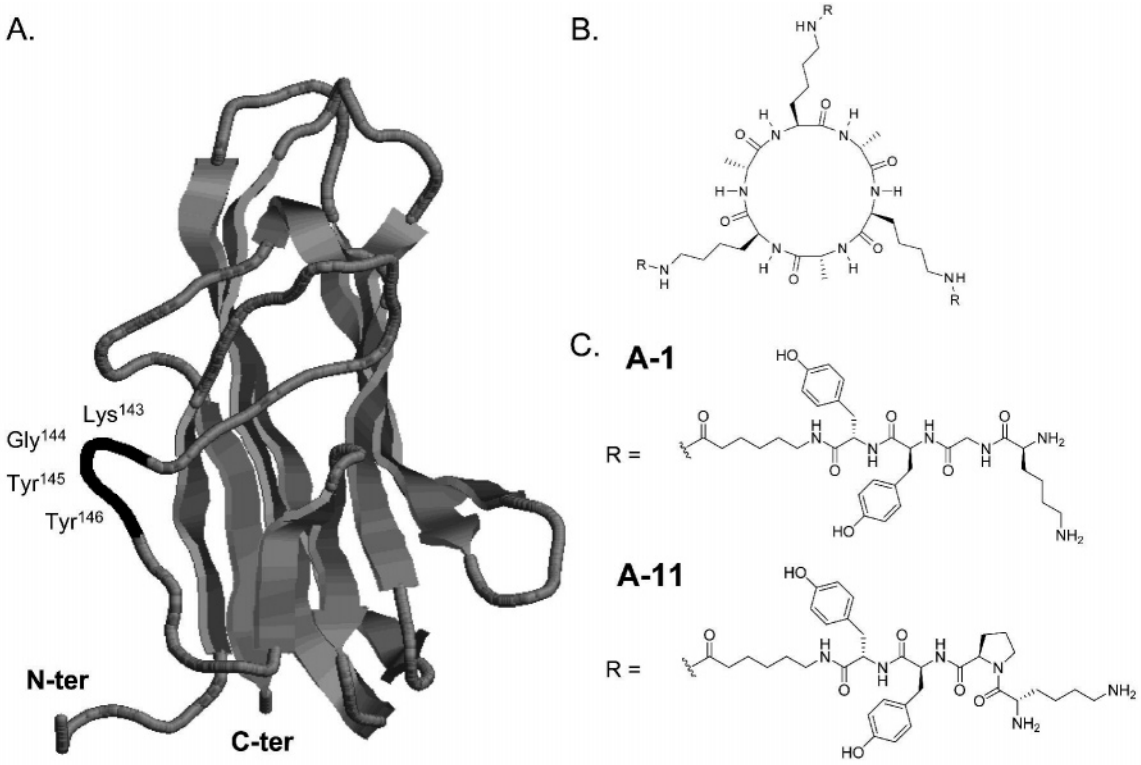

FIGURE 1: Synthetic homotrimeric CD40L mimetics. (A) Representation at atomic resolution of the human CD40L extracellular domain fragment (PDB entry 1ALY) (*25*). The CD40-binding motif (Lys^{143}-Gly^{144}-Tyr^{145}-Tyr^{146}) in the AA″ loop considered for the design CD40L mimetics is colored black. (B) Trimeric **A-1** and **A-11** molecules were synthesized by a fragment coupling CD40-binding pentapeptide (C) to the macrocyclic C_3-symmetric D,L-α-hexapeptide core as previously described (*32*). In the case of **A-11**, the glycyl residue from the binding motif of **A-1** was substituted for the non-natural D-prolyl residue.

version 3.3 (Becton Dickinson, Pont de Claix, France), and the data were processed with WinMDI version 2.8 (J. Trotter, Scripps Research Institute, La Jolla, CA).

Western Blotting. Total cellular extracts were prepared by treatment in lysis buffer [50 mM Tris-HCl (pH 7.4), 300 mM NaCl, 10% glycerol, 0.5% Triton X-100, 2 mM EDTA, 2 mM activated-sodium orthovanadate, and protease inhibitor cocktail (Sigma Aldrich)] for 20 min on ice. Lysates were clarified by centrifugation at 10000*g* for 20 min at 4 °C and quantified for total protein concentration with the bicinchoninic acid assay (BCA, Pierce, Rockford, IL). Ten micrograms of total cellular proteins was separated by 10% SDS−polyacrylamide gel electrophoresis (PAGE) and transferred to a nitrocellulose membrane. The membrane was saturated with Tris-buffered saline (TBS) containing 0.5% (w/v) Tween 20 (TBS-T) and 5% (w/v) nonfat milk (TBS-T/milk) for 1 h at room temperature and then incubated overnight at 4 °C with the anti-IκB-α or anti-actin antibody diluted 1:2000 in TBS-T/milk. After three washes with TBS-T at room temperature, the membrane was incubated at room temperature for 1 h with the GAR or GAM antibody diluted 1:5000 in TBS-T/milk. After three washes with TBS-T, the membrane was incubated with ECL reagent (Amersham), and the relative signal intensity of each band was quantified by densitometry with the gel analyzer tool from ImageJ version 1.37f (http://rsb.info.nih.gov/ij/) after scanning of the radiography.

Comparative Reverse Transcription Polymerase Chain Reaction (RT-PCR). Expression of the *IL-12 p40* messenger RNA (mRNA) was evaluated by comparative RT-PCR as described previously (*32*). Total RNA was isolated from D1 cells with TriReagent-LS (Molecular Research Center, Inc., Cincinnati, OH) and converted to complementary DNA (cDNA) with Moloney-Murine leukemia virus reverse transcriptase (Sigma Aldrich) according to the manufacturer's instructions. The primers used to amplify *IL-12 p40* cDNA were as follows: forward, 5′ GGA AGC ACG GCA GCA GAA TA 3′; reverse, 5′ AAC TTG AGG GAG AAG TAG GAA TGG 3′.

As a constant probe, the cDNA sequence of the housekeeping gene glyceraldehyde phosphate dehydrogenase (*Gapdh*) was also amplified using the following primers: forward, 5′ CGT CCC GTA GAC AAA ATG GTG 3′; reverse, 5′ GTG GAT GCA GGG ATG ATG TTC 3′.

The sizes of the amplified products were 180 bp for *IL-12 p40* and 642 bp for *Gapdh*. A thermal cycle of 30 s at 94 °C, 45 s at 56 °C, and 45 s at 74 °C was used 26−32 times for *IL-12 p40* and 16−22 times for *Gapdh* using the Taq DNA polymerase (Promega, Madison, WI) according to the manufacturer's instructions. Five microliters of each amplicon was taken from the exponential phase of the PCR (set up before each test) and analyzed by electrophoresis on a 1% agarose gel in a 10 mM sodium borate, 2 mM EDTA, and 2 μg/mL ethidium bromide buffer. Imaging data of the ethidium bromide-stained amplified products were obtained with the ChemiDoc XRS system (Bio-Rad, Hercules, CA) using Quantity One.

Statistical Analysis. The one-tailed Student's *t*-test tool from the statistical package of Microsoft Excel 10 was used to analyze data for significant differences. p values of <0.05 were regarded as significant. SigmaPlot 6.00 (SPSS Inc., Chicago, IL) was used for linear regression analysis of Hill

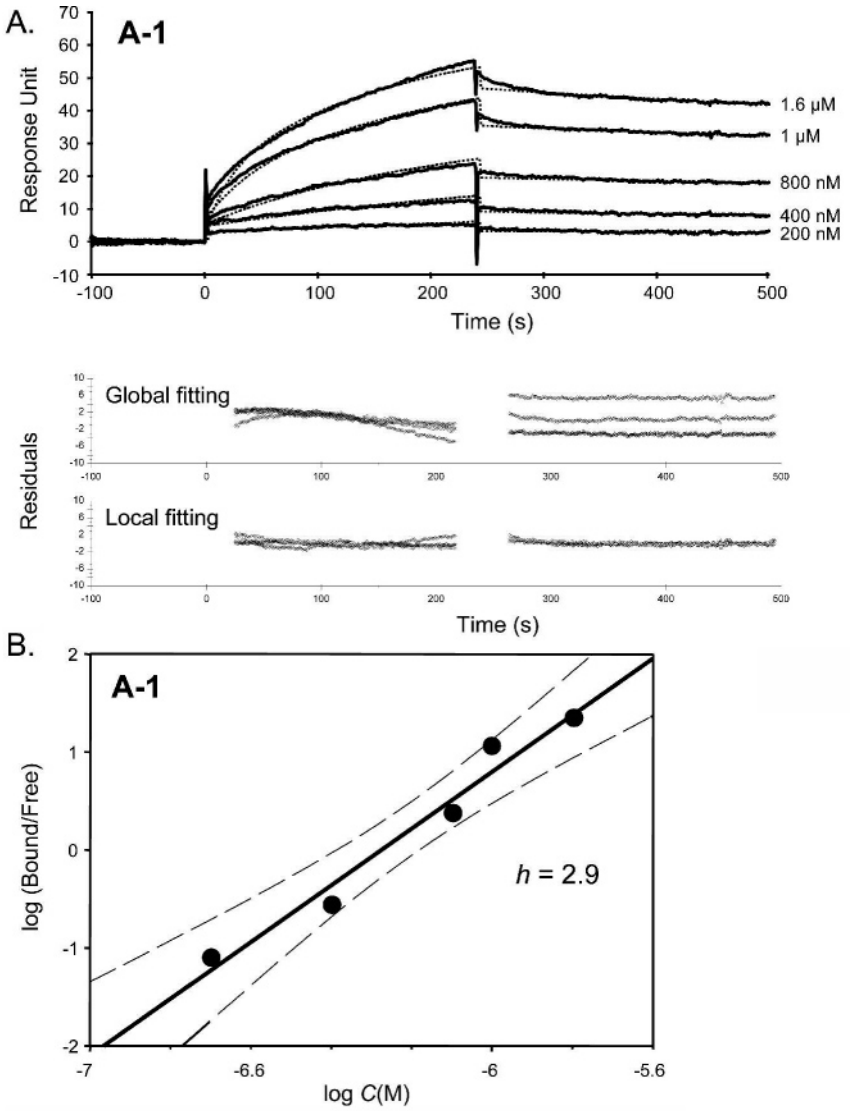

FIGURE 2: SPR experiments, fitting methods, and analysis of cooperativity for **A-1** binding. Study of the direct binding of mini-CD40L **A-1** to captured rshCD40−mIg, as shown by SPR. (A) The top graph represents the binding data for **A-1** at the indicated concentrations (solid lines) and the fitting curves (dashed lines) using the trivalent model with rate constants for the first binding event determined by local fitting. The bottom graphs represent the residuals for the fitting from the trivalent analyte model in global (global fitting) or local (local fitting) mode. One experiment representative of three is shown. (B) Hill representation for **A-1** binding using data extracted from sensorgrams of the experiment shown in panel A. Bound and Free denote R_{eq} and the difference $R_{max} - R_{eq}$, respectively. *C* denotes the concentration of CD40 ligand injected. The Hill number *h*, assessed by linear regression, is given for each mimetic, and 95% confidence intervals are shown (− − −).

curves and determination of confidence intervals, that is regions where any given data point will fall with 95% probability a certain distance from the regression line.

RESULTS

Design of the Mini-CD40Ls. Like other members of the TNFR superfamily, CD40L assembles into C_3-symmetric complexes forming stoichiometrically defined homotrimers. On the basis of the X-ray structure of the human CD40L extracellular domain (Figure 1A), and using a model of the CD40−CD40L interaction as well as data obtained from previous site-directed mutagenesis studies (*41*), we previously designed trimeric CD40L mimetics, named mini-CD40Ls. We synthesized a CD40-binding motif fragment containing hot spot residues from the AA″ loop (Lys^{143}, Tyr^{145}, and Tyr^{146}; Figure 1A, black residues) and coupled it to a rigid flat macrocyclic scaffold (Figure 1B), chosen for an optimal trimeric radial distribution (*32*), via an aminohexanoic acid (Ahx) residue spacer (Figure 1C). These conditions in length and geometry were necessary for the proper functional mimetism of CD40L, and the first active molecule was named **A-1** (Figure 1C). Detailed analysis of the AA″ loop in the crystal structure of CD40L (Figure 1A, black residues) reveals a turnlike geometry centered on the Gly^{144} and Tyr^{145} residues with ϕ_{i+1}, ψ_{i+1}, and ϕ_{i+2} angles close to those of an ideal type II′ β turn (*42*). We have previously shown that Gly^{144}, in contrast to Lys^{143}, Tyr^{145}, and Tyr^{146}, can be substituted with Ala without any significant effect on the functional properties of mini-CD40L **A-1** (*32*). Herein, to better mimic the turn geometry adopted by the CD40-binding segment in the structure of CD40L, we decided to fix the ϕ_{i+1} and ψ_{i+1} angles by replacing the glycyl residue with the non-natural D-prolyl one (*43*). The analogous molecule obtained was named **A-11** (Figure 1C).

Table 1: Summary of Measured Kinetic Binding Parameters and Affinity Constants for the Interaction of CD40L Mimetics **A-1** and **A-11** with Captured rshCD40−mIg As Determined by SPR[a]

(A) Local Fitting

	CD40L mimetic	k_{a1} (M^{-1} s^{-1})	k_{d1} (s^{-1})	k_{a2} (RU^{-1} s^{-1})	k_{d2} (s^{-1})	k_{a3} (RU^{-1} s^{-1})	k_{d3} (s^{-1})	K_{D1} (nM)	overall k_d (s^{-1})	overall K_D (nM)	R_{max}	χ^2
trivalent model	**A-1**	$(3.8 \pm 2.8) \times 10^3$	$(1.5 \pm 1.1) \times 10^{-3}$	2.9×10^{-3}	0.13	5.1×10^{-3}	0.055	395	$(6.8 \pm 3.2) \times 10^{-4}$	179	67.4	0.43
	A-11	$(2.8 \pm 0.7) \times 10^3$	$(1.1 \pm 0.3) \times 10^{-3}$	2.8×10^{-4}	0.03	3.5×10^{-7}	5.3×10^{-3}	393	$(6.7 \pm 1.6) \times 10^{-4}$	239	170	1.5

	CD40L mimetic	k_a (M^{-1} s^{-1})	k_d (s^{-1})	K_D (nM)	R_{max}	χ^2
1:1 model	**A-1**	$(3.3 \pm 1.8) \times 10^3$	$(4.0 \pm 2.7) \times 10^{-4}$	121	52.4	0.85
	A-11	$(3.5 \pm 0.9) \times 10^3$	$(6.4 \pm 2.8) \times 10^{-4}$	183	131	1.62

(B) Global Fitting

	CD40L mimetic	k_{a1} (M^{-1} s^{-1})	k_{d1} (s^{-1})	k_{a2} (RU^{-1} s^{-1})	k_{d2} (s^{-1})	k_{a3} (RU^{-1} s^{-1})	k_{d3} (s^{-1})	K_{D1} (nM)	overall k_d (s^{-1})	overall K_D (nM)	R_{max}	χ^2
trivalent model	**A-1**	175	3.03×10^{-4}	1.2×10^{-9}	7.0×10^{-4}	7.5×10^{-8}	1.5×10^{-3}	1731	4.72×10^{-4}	2697	733	8.38
	A-11	966	0.016	1.4×10^{-5}	1.2×10^{-3}	6.1×10^{-4}	1.4×10^{-3}	16200	7.9×10^{-4}	818	790	15.7

	CD40L mimetic	k_a (M^{-1} s^{-1})	k_d (s^{-1})	K_D (nM)	R_{max}	χ^2
1:1 model	**A-1**	124	5.1×10^{-5}	412	965	8.42
	A-11	1.8×10^3	8.6×10^{-4}	457	212	16.4

[a] The data from Figures 2A and 3A were evaluated with the indicated binding model. The first binding events in the trivalent model are means ± SD of the rate constants obtained for all the concentrations. Overall k_d values were determined as means of all the observed dissociation rate constants. Overall K_D = (overall k_d)/k_{a1}. $K_{D1} = k_{d1}/k_{a1}$.

*Analysis of the Binding of Mini-CD40L **A-1** to CD40 by SPR.* We have previously shown that **A-1** (i) effectively inhibits the binding of rshCD40L−mCD8 to a rshCD40−mIg captured on a RAM-coated CM5 chip, (ii) directly binds to CD40, and (iii) interacts with a CD40 molecule captured by an anti-CD40 Ab (*32*). Our present SPR data fit better with a trivalent model (Figure 2A) than with the classical Langmuir 1:1 monovalent one, suggesting that this interaction is of one mini-CD40L for three CD40 receptors. Fitting was only correctly achieved by using a local fitting instead of a global fitting of the rate constants for the first binding event, that is, k_{a1} and k_{d1}, with χ^2 falling from 8.42 to 0.85 for the 1:1 model (Table 1). Indeed, global fitting resulted in R_{max} values too high to be stoichiometrically correct based on the molecular mass of ca. 3000 Da for each mini-CD40L and the level of CD40 captured (approximately 450 RU in all the experiments, with a predicted molecular mass of 45.6 kDa for a monomer). Local fitting using a trivalent model instead of a monovalent model resulted in χ^2 values of 0.43 and 0.85, respectively, suggesting a better fit with the trivalent model. The binding of **A-1** to CD40 is thus better explained by a multistep interaction in which the first CD40-binding motif interacts with a CD40 molecule and then the second and third peptides of **A-1** bind to two other CD40 molecules. This is probably due to the radial distribution of the pentapeptides from the rigid core, the flexibility of the spacer arms, and the three-dimensional context created by a multilayer CD40 presentation on a carboxylated dextran chip.

*Cooperativity of the Binding of Mini-CD40L **A-1** to CD40.* The discrepancy between the result obtained by global fitting and that from local fitting prompted us to consider a more complex interaction. Kinetic data obtained from the fitting described above were used to assess the cooperative level of the interaction, assuming that the mimetics are trivalent and the CD40 is distributed in a cell membrane-like context. Interaction between the Fc domains of the chimeric CD40−Ig construct, Brownian diffusion of the injected molecules, and the apparent flexibility of their spacer arms could explain a cooperative effect by which the binding of the first recognition element of the trivalent ligand enhances the binding of the other ones to monomeric CD40 molecules. This mechanism should be easily described by a SPR technique, which permits us to record binding of a nontagged molecule to another captured one in real time and in a reconstituted three-dimensional lattice. The Hill plot is a method of analyzing the cooperativity. It requires data at equilibrium to assess the fractionated saturation, denoted *Y*, of the binding sites in relation to the concentration of multimeric molecules. Unfortunately, the equilibrium could never be reached (data not shown) probably because nonspecific interactions between bound and free analyte molecules with very low association rates are interfering. Since SPR measures changes in mass on the chip, only the R_{eq} after the first binding event is important. Indeed, subsequent kinetics alter the form of the binding curve but not the intensity of the signal. We thus extracted equilibrium values from kinetic rate constants for the first binding event and used them to trace the Hill plot for each ligand (eqs 1−5 from Materials and Methods; see also Surface plasmon resonance analysis; summary of the equations used for the determination of kinetics data in the Supporting Information). These plots indicated that the **A-1**−CD40 interaction was cooperative with an *h* of 2.9 (Figure 2B). We can notice that the rshCD40L−mCD8 molecule has the same cooperative property (Figure S1 of the Supporting Information), confirming that it naturally homotrimerizes in solution to give fully functional homotrimeric CD40L as shown by other groups (*5*).

Effect of the Gly^{144} → D-Pro Mutation on the Binding of Mini-CD40Ls to CD40. We compared the binding of **A-11** to CD40 under the same conditions and fitted the experimental curves with the same models as described above (Table 1). Here again, global fitting was avoided since χ^2 values shifted from 16.4 and 15.7 to 1.62 and 1.50 for the

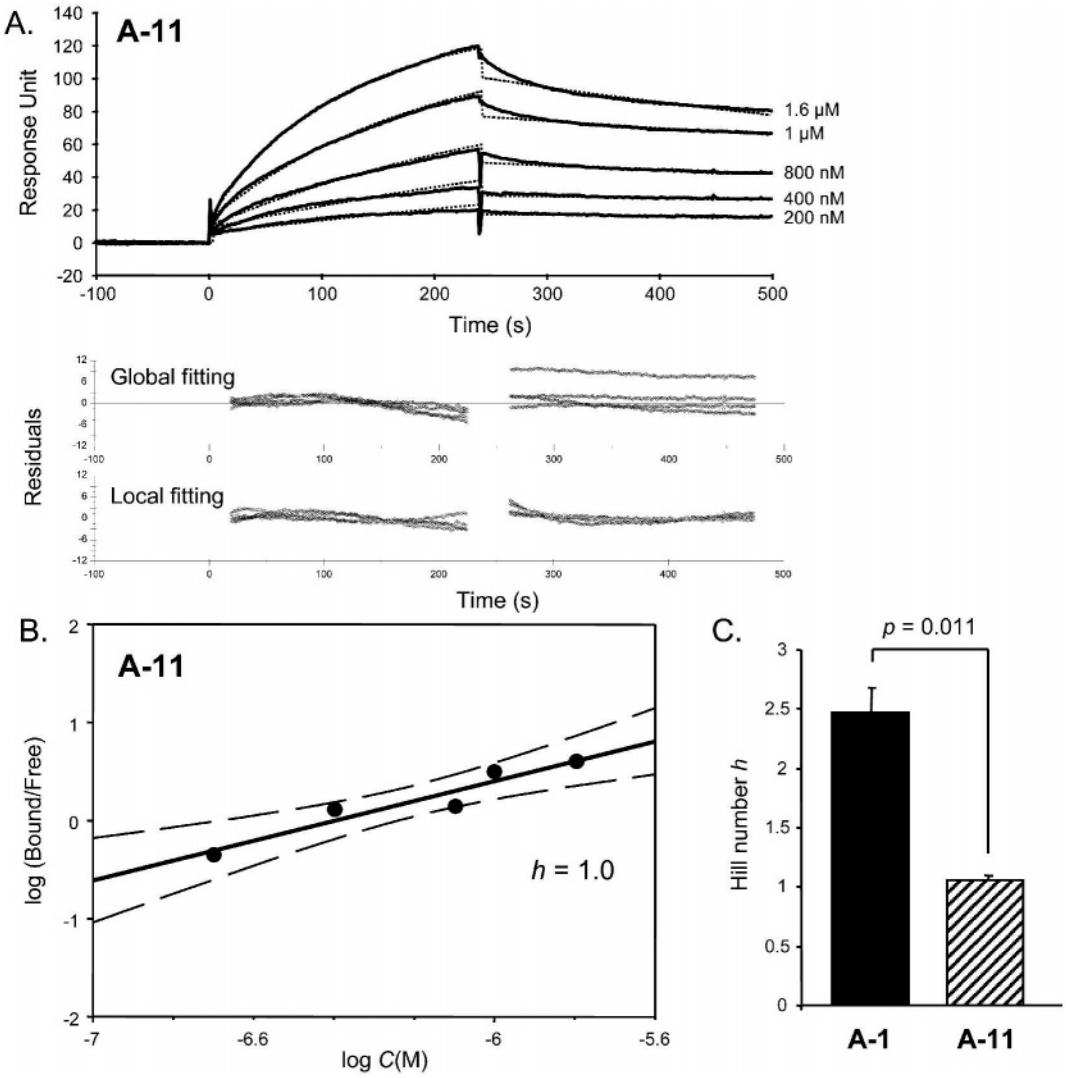

FIGURE 3: Effect of the Gly^{144} → D-Pro mutation in the CD40-binding motif on the binding of mini-CD40Ls. Study of the direct binding of mini-CD40L **A-11** to captured rshCD40−mIg as in Figure 2. (A) The top graph represents the binding data for **A-11** at the indicated concentrations (solid lines) and the fitting curves (dashed lines) using the trivalent model with rate constants for the first binding event determined by local fitting. The bottom graphs represent the residuals for the fitting from the trivalent analyte model in global (global fitting) or local (local fitting) mode. One experiment representative of three is shown. (B) Hill representation for **A-11** using data extracted from sensorgrams from panel A. Bound and Free denote R_{eq} and the difference $R_{max} - R_{eq}$, respectively. *C* denotes the concentration of CD40-ligand injected. The Hill number *h*, assessed by linear regression, is given for each mimetic, and 95% confidence intervals are shown (− − −). (C) Means ± SE of the *h* values from three independent experiments, with two different batches of mini-CD40Ls **A-1** and **A-11**, determined by the same method and under the same conditions. *p* was determined with a Student's *t*-test.

monovalent and trivalent models, respectively, comparing global and local fitting. Rate constants are in the order of the ones measured for **A-1** with the use of the monovalent model. The R_{max}, however, differed, suggesting a difference in stoichiometry between the two mini-CD40Ls. Indeed, the maximum binding capacity for **A-11** is 2.5-fold greater than the R_{max} value obtained for **A-1**, whatever model was used (Figures 2A and 3A). As the R_{max} for **A-1** mathematically better corresponds to a 1:3 stoichiometry, and when we take into account the fact that χ^2 in local fitting cannot distinguish between a monovalent and a trivalent mechanism, our data suggest that **A-11** rather binds to CD40 in a monovalent manner. Nevertheless, the local fitting resulted in a χ^2 lower than the global one, probably because a change in valency as a function of the **A-11** concentration is not reflected in the global model. Due to a higher dissociation rate constant for the first CD40-binding motif (Table 1), equilibrium is shifted toward monovalent interactions at high concentrations. Hill plots were calculated as explained for **A-1**. The trivalent model was preferred for comparison with **A-1** binding results and takes into account any cooperative effect at low concentrations of **A-11** at which multivalent interactions may occur. As expected, the loss of trivalency has led to a loss of cooperativity for **A-11** from which a Hill coefficient of 1.0 was calculated (Figure 3B). The experiments were repeated twice under similar conditions, with two different batches of each of the mini-CD40Ls, to confirm that the replacement of the glycyl residue with a D-prolyl residue in the CD40 motif did not affect the binding of the molecule to CD40 (Table 1 and Figures 2A and 3A) but led to the significant ($p = 0.011$) loss of cooperativity with Hill numbers of 2.4 ± 0.2 for **A-1** and 1.0 ± 0.04 for **A-11** (Figure 3C).

Effect of the Gly^{144} → D-Pro Mutation on the Pro-Apoptotic Properties of Mini-CD40Ls on B Lymphoma Cells. The two CD40 ligands **A-1** and **A-11** were compared for

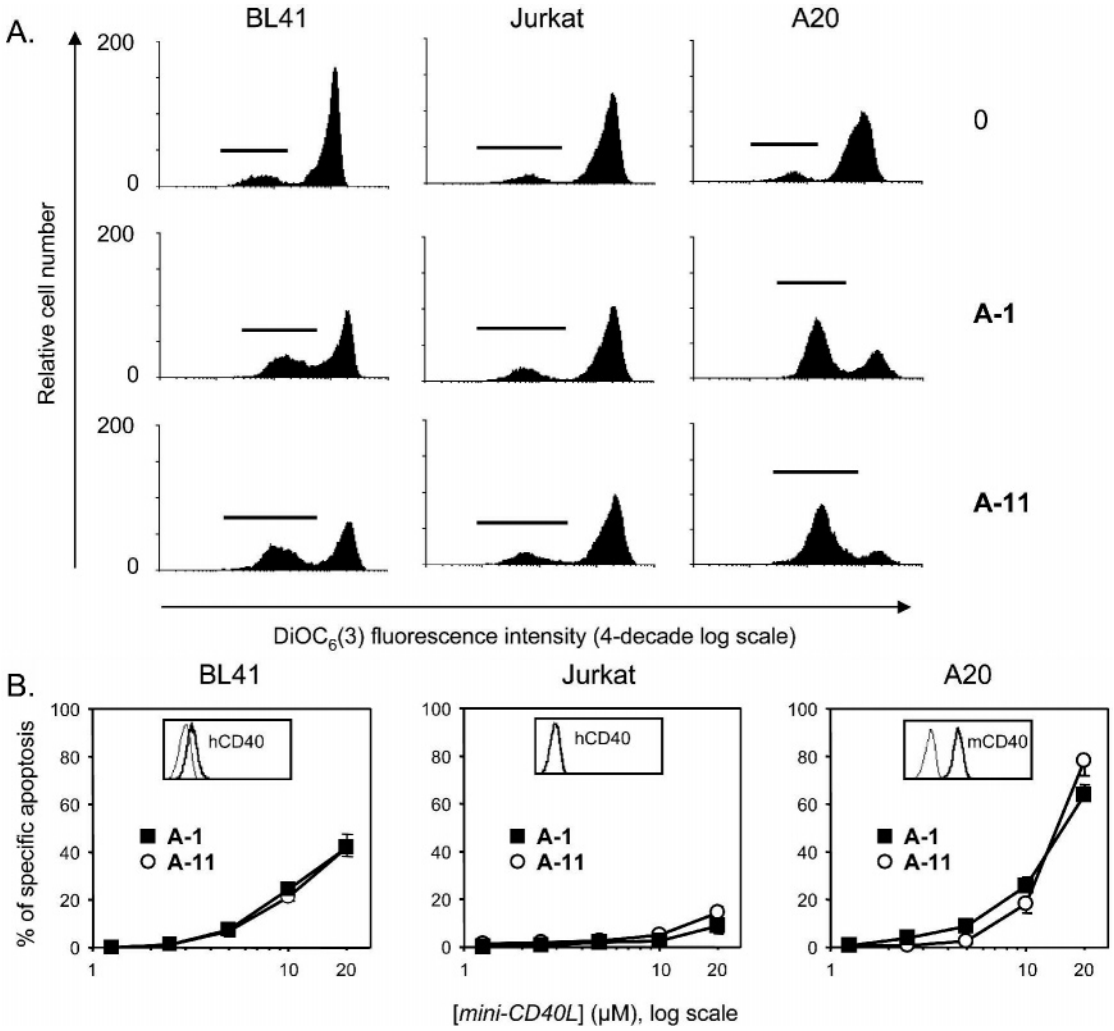

FIGURE 4: Effect of the Gly^{144} → D-Pro mutation in the CD40-binding motif on the induction of apoptosis of human and mouse lymphoma cells. Induction of apoptosis assessed by the decrease in $\Delta\psi_m$, as detected by a reduction in the rate of $DiOC_6(3)$ dye uptake. (A) A representative panel of the $DiOC_6(3)$ staining of BL41, Jurkat, and A20 cells, not treated (0) or treated with **A-1** or **A-11** at 20 μM for 16 h. (B) Effect of **A-1** (■) and **A-11** (○) on human B lymphoma BL41, human T leukemia Jurkat, and mouse B lymphoma A20 cells after incubation for 16 h. Levels of membrane expression of the human and mouse CD40 protein as measured by flow cytometry are shown in the inset. Results are expressed as the averages ± SE of three independent experiments with two different batches of each mimetic.

their biological effects in several cell-based assays. Differences in their functional behavior could tentatively be correlated to the loss of cooperativity observed in the SPR context. Caution must nevertheless be exercised because the distribution of CD40 molecules at the surface of the sensor chip may differ from that at the cell membrane in several aspects such as density, accessibility, fluidity, and preorganization. We first used the property of Burkitt lymphoma cells to engage apoptosis after ligation of CD40 with its cognate ligand (*31*). The BL41 human B lymphoma cells expressing CD40 (Figure 4B, insets) were incubated with different concentrations of each mini-CD40L for 16 h, and apoptosis was then assessed by flow cytometry with the $DiOC_6(3)$ dye, probing the decrease in mitochondrial membrane potential (Figure 4A) consecutive to induction of apoptotic pathways. The two mimetics induced apoptosis of BL41 cells with no significant differences (Figure 4A,B). In contrast, neither of them was efficient on Jurkat human leukemia cells, which do not express CD40. This was comparable to the effects induced by rshCD40L−mCD8 (data not shown) and emphasized the specificity toward CD40. Finally, because of the cross reactivity of murine CD40L toward human and murine CD40 (*32*, *44*), the mouse B lymphoma cell line A20 expressing murine CD40 (Figure 4B, inset) was tested against the two ligands, and no significant differences were observed in the level of apoptosis they induced (Figure 4A,B).

Effect of the Gly^{144} → D-Pro Mutation on the Maturation of Mouse Dendritic Cells. In contrast, engagement of CD40 by the two mini-CD40Ls in the D1 mouse dendritic cell line (*45*) resulted in a differential functional outcome. We have already shown that **A-1** efficiently induced the maturation of D1 cells by increasing the level of expression of costimulatory proteins such as CD80 (B7-1), CD86 (B7-2), CD54 (ICAM-1), and IA^b and by overexpressing CD40 itself (*32*). As shown in Figure 5A (top panel), **A-1** induced maturation of more than 90% of the cells from a 5 μM solution after incubation for 24 h. In contrast, the expression level of the maturation markers was significantly lower in the presence of **A-11**, and even if we detected nearly 50% of the cells expressing a higher level of CD86 at 10 μM compared to the nontreated cells, the efficiency never reached that of **A-1** at lower concentrations (Figure 5A, bottom panel). A more complete study of the degree of overexpres-

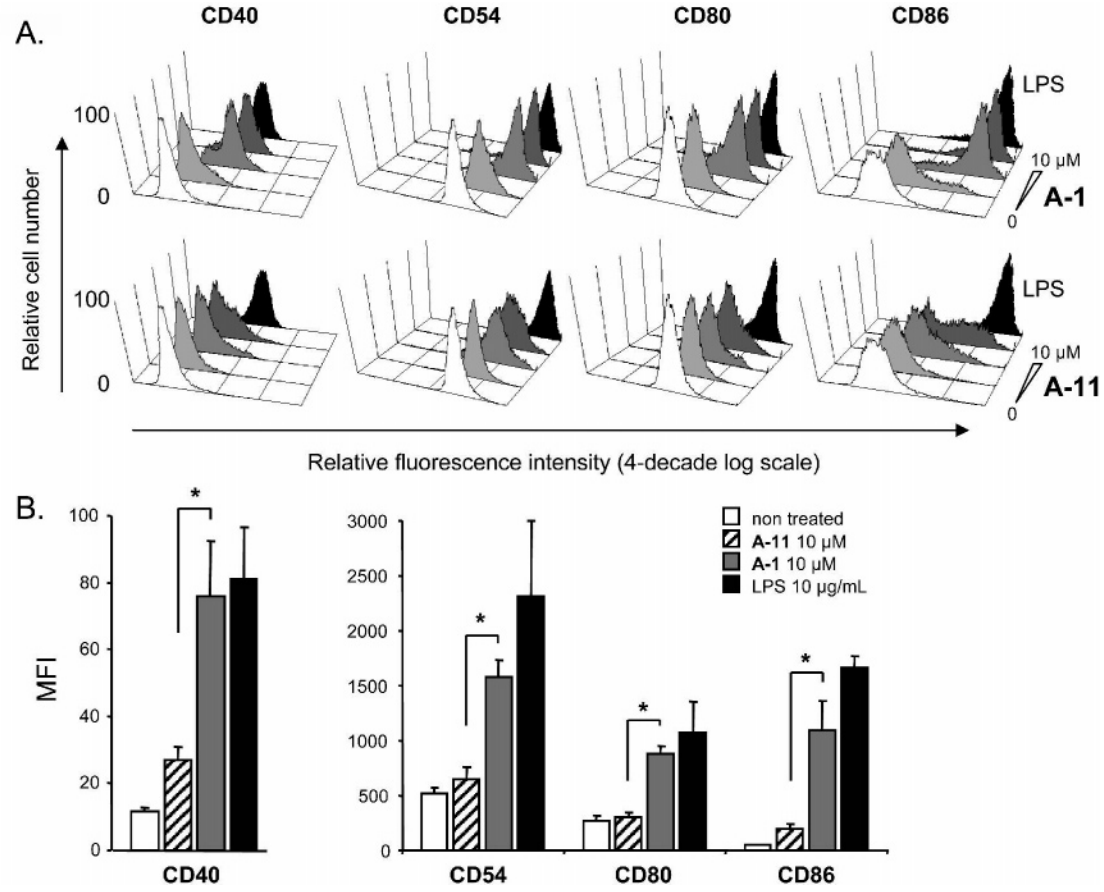

FIGURE 5: Effect of the Gly^{144} → D-Pro mutation in the CD40-binding motif on the maturation of the D1 mouse dendritic cell line. (A) Expression of maturation markers, as measured by flow cytometry after treatment for 24 h with **A-1** (top line) or **A-11** (bottom line) with increasing concentrations of mini-CD40L (light, medium, and dark gray histograms for 2.5, 5, and 10 μM, respectively). Empty histograms represent nontreated cells and full histograms cells treated with LPS at 10 μg/mL (positive control). One experiment representative of three independent experiments with two different batches of each ligand is shown. (B) MFIs after treatment for 24 h with the mini-CD40Ls were measured by flow cytometry for each of the maturation markers. Empty, dashed, gray, and black bars represent nontreated samples, **A-11** at 10 μM, **A-1** at 10 μM, and LPS, respectively. Averages ± SE of three independent experiments with two different batches of each mimetic are shown. An asterisk denotes a p of <0.05 (Student's t-test) between treatment with **A-1** and **A-11**.

sion for each of these maturation markers was conducted in three independent experiments by using two different batches of mini-CD40Ls, and the mean fluorescence intensity (MFI) was measured after incubation for 24 h (Figure 5B). When **A-1** at 10 μM reached the saturated expression level of LPS-stimulated cells for every marker, **A-11** effects were not comparable to the **A-1** activity for all of the maturation markers that were tested ($p < 0.05$). Even if MFI cannot be neglected in the case of CD40 and CD86 markers, **A-11** has largely lost its activity toward maturation of these dendritic cells.

Effect of the Gly^{144} → D-Pro Mutation on the Signaling Induced in the Mouse Dendritic Cells. Finally, we measured the level of *IL-12 p40* mRNA, another marker of CD40L stimulation. Interestingly, both **A-11** and **A-1** induced the transcription of this cytokine subunit (Figure 6A), pointing out the efficient engagement of common pathways by the two mini-CD40Ls from CD40 in these cells. To understand the mechanisms involved in the differential effect induced by **A-11**, we investigated the ability of the two CD40L mimetics to induce the degradation of IκB-α, a step necessary for the subsequent translocation of NF-κB to the nucleus (*46*). As previously described, **A-1** induced a net degradation of IκB-α in a dose−response manner after incubation for 45 min. By contrast, **A-11** failed to induce any effect (Figure 6B), even after incubation for 6 h at 10 μM (Figure 6C).

DISCUSSION

The CD40−CD40L interaction is a key event for the activation of both the cellular and humoral immune responses. A broad range of CD40 cellular expression has been described on immune and non-immune cells and on various cancer cells like lymphoma cells. However, the relation between the various effects resulting from CD40 activation in this large cells network is still lacking because signaling pathways vary from cell to cell (*47*). Indeed, the intracellular events mostly studied on B cells are complex and are regulated by diverse environmental and intracellular agents, resulting in differential biological effects. For instance, CD40 activation in malignant B cells results in growth inhibition instead of differentiation in nontransformed B cells (*18*). Tools for studying the induction of different regulatory pathways are missing. Here we show that a one-residue mutation in the receptor-binding motif of our CD40L mimetics led to a variation in their physicochemical properties and, more importantly, to a selective deactivation of an intracellular signal.

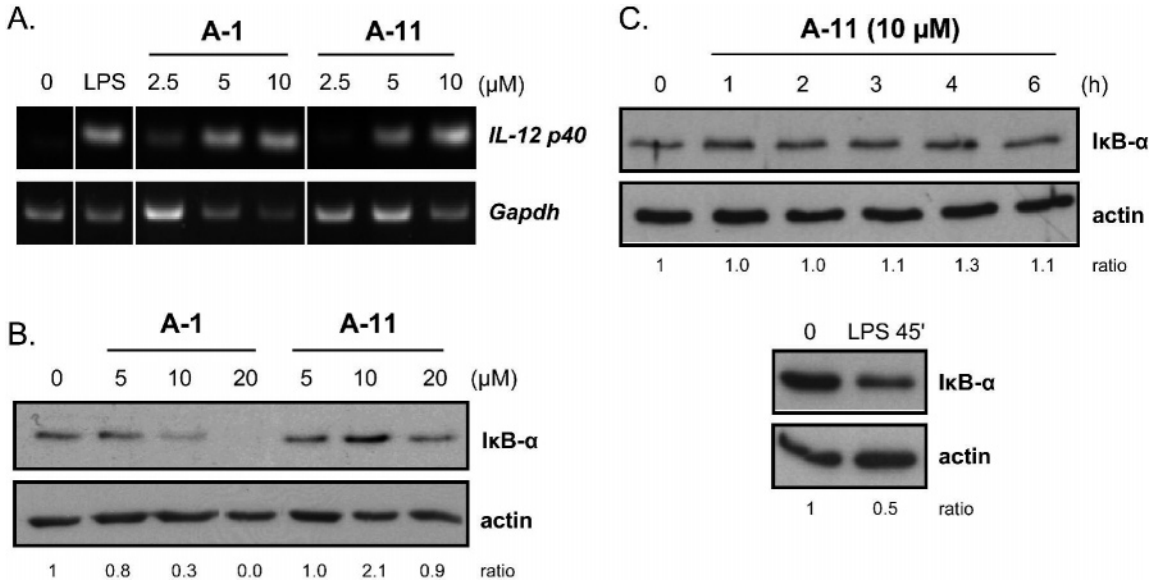

FIGURE 6: Effect of the Gly^{144} → D-Pro mutation in the CD40-binding motif on the signaling induced in the D1 mouse dendritic cell line. (A) Induction of *IL-12 p40* mRNA transcription by **A-1** and **A-11** as measured by comparative RT-PCR after treatment for 16 h. *Gapdh* was used as a housekeeping gene control. (B) Induction of the NF-κB pathway by **A-1** and **A-11**. D1 cells were treated for 45 min with the indicated concentration of the CD40L mimetic. IκB-α degradation was then assessed by immunoblotting on cell extracts, and actin was used as an internal loading control. The ratio of the band intensity of IκB-α to that of actin is given under each lane. (C) Kinetics of activation of the NF-κB pathway as measured by immunoblotting of IκB-α. D1 cells were treated with **A-11** at 10 μM for the indicated times or with LPS at 10 μg/mL for 45 min. The ratio of the band intensity of IκB-α to that of actin is given under each lane.

The rationale behind the chemical modification was to stabilize the naturally occurring β turn-type geometry found in the CD40-binding motif of the CD40L homotrimer. We changed the glycyl residue in the three Lys-Gly-Tyr-Tyr-Ahx pentapeptides linked onto the C_3-symmetrical core of mini-CD40L **A-1**, for the non-natural D-prolyl residue stabilizing a conformation closer to the native structure. The D-prolyl-modified molecule lost its capacity to bind CD40 in a cooperative manner. While the discrepancy between global and local fitting of the data on **A-1** binding is probably due to its cooperative character, for **A-11** it might be due to a change in stoichiometry. Indeed, at low concentrations, the molecule probably binds in a 3:1 or 2:1 ratio, but since the multivalent binding is not stabilized by a cooperative process, at high concentrations only the dimeric complex is formed, explaining the stoichiometry. We suggest that the Gly^{144} → D-Pro modification has rigidified the binding motif, lowering its capacity to induce allosteric movements. Two alternatives are envisaged to explain why the first event of binding of **A-1** enhances the binding of the second and third binding motifs to CD40. Ligand restructuring occurs and allows faster subsequent interactions with the receptor. Alternatively, some allosteric movements in the tetravalent complex make the second and third CD40 molecules more susceptible to subsequent interactions. Indeed, the rshCD40−mIg construct seems to oligomerize as assessed by electrophoresis under nonreducing conditions (data not shown). Anyway, our experimental data cannot discriminate between the two alternatives, although a lack of cooperativity by **A-11** makes the first alternative more likely. The difference in the binding behavior of the two molecules did not alter their property to induce apoptosis in B cell lymphoma cells. However, we found a different biological behavior between the two mini-CD40Ls in maturation of the D1 mouse dendritic cell line, and only **A-1** upregulated costimulatory molecules. This effect was correlated with the inability of **A-11** to induce NF-κB activation. We showed further that despite these different effects, both of the mimetics stimulated production of *IL-12 p40* mRNA, suggesting not a complete loss of the effect on a particular cell but the engagement of different intracellular signals.

These results can be linked to a recent study of the complex regulation of CD40-mediated signaling (*48*) in which the authors showed that the p38 mitogen-activated protein kinase (MAPK) and the alternative NF-κB pathways are selectively activated depending on the maturation status of the DC. In particular, they demonstrated that a p38 MAPK inhibitor downregulated the production of the CD40-mediated IL-12 protein by immature DCs but showed no significant effects on mature cells. Furthermore, Mackey et al. (*49*) have isolated separated pathways engaged from the CD40 receptor in primary DC by mutation of the binding sites for the different TRAFs in the receptor cytoplasmic domain. They showed independent signaling engagement for TRAF 2, 3, and 5, and for TRAF 6, and in particular, they showed that only disruption of the binding of TRAF 6 to CD40 markedly decreases the level of *IL-12 p40* secretion along with p38 MAPK and JNK activation in response to CD40L. These observations, our results, and the well-known complex signalosome organization in the membrane rafts of DC (*29*) lead us to propose a more complex mechanism behind the pattern of downstream signals. The 3:3 stoichiometry between CD40 and its ligand is essential for the recruitment of the required complex under the membrane for the initiation of a downstream signal. However, due to the context of some membrane microdomains, the close communication between other trivalent receptor molecules would orient the cascades to be activated. For example, TRAF recruitment would greatly vary depending on the density of CD40 at the membrane. A specific matrix for the placement of submembrane partners, in which some binding sites are more or less accessible, would modulate this

organization and leads to the activation of different pathways. This could explain the results of Yanagawa et al. (*48*) since CD40 is overexpressed in mature DCs compared to immature cells, but also the discrepancy observed among CD40L soluble protein, membranous CD40L, and antibody directed against CD40. A molecular consequence would be the inability to form microaggregates, as shown by Legembre et al. for Fas (*50*), another member of the TNFR family. In this model, an apoptotic signal could be sent without formation of SDS-stable and reducing agent-resistant microaggregates. In fact, both the anti-Fas agonist Ab and multimeric soluble FasL lead to Fas oligomerization and subsequent apoptosis of normal lymphocytes, but only the Ab stabilizes it inside microaggregates, triggering pathways that are subtly different.

The CD40-binding motif rigidification induced by the $Gly^{144} \rightarrow$ D-Pro modification does not lead to a complete loss of activity. The **A-11**−CD40 complexes probably do not allow formation of microaggregates, leading to a different submembranous organization or stability and initiating different intracellular signals.

Finally, mini-CD40Ls could be valuable tools for dissecting the mechanisms set up during ligand−receptor interaction and analyzing the multireceptor signaling complexes engaged in downstream cellular events following CD40 activation.

ACKNOWLEDGMENT

We thank our colleagues at the laboratoire d'Immunologie et Chimie Thérapeutiques for continuous interest and insightful discussions, in particular, A. Bianco and P. Eftekhari for critical reading of the manuscript, J.-P. Briand and S. Muller for continuous support; N. Bonnefoy-Berard and M. Flacher for providing the lymphoma cells, C. J. M. Melief for providing the D1 dendritic cell line, M. Monestier for providing the LG11-2 hybridoma, and P. Schneider for suggesting the name "mini-CD40L" for our synthetic CD40L mimetics.

SUPPORTING INFORMATION AVAILABLE

Surface plasmon resonance (SPR) analysis, summary of the equations used for the determination of the kinetic data, and SPR experiments and analysis of cooperativity for the rshCD40L−mCD8 protein (Figure S1). This material is available free of charge via the Internet at http://pubs.acs.org.

REFERENCES

1. Bodmer, J. L., Schneider, P., and Tschopp, J. (2002) The molecular architecture of the TNF superfamily, *Trends Biochem. Sci. 27*, 19−26.
2. Armitage, R. J., Fanslow, W. C., Strockbine, L., Sato, T. A., Clifford, K. N., Macduff, B. M., Anderson, D. M., Gimpel, S. D., Davis-Smith, T., Maliszewski, C. R., et al. (1992) Molecular and biological characterization of a murine ligand for CD40, *Nature 357*, 80−82.
3. Noelle, R. J., Roy, M., Shepherd, D. M., Stamenkovic, I., Ledbetter, J. A., and Aruffo, A. (1992) A 39-kDa protein on activated helper T cells binds CD40 and transduces the signal for cognate activation of B cells, *Proc. Natl. Acad. Sci. U.S.A. 89*, 6550−6554.
4. Lane, P., Brocker, T., Hubele, S., Padovan, E., Lanzavecchia, A., and McConnell, F. (1993) Soluble CD40 ligand can replace the normal T cell-derived CD40 ligand signal to B cells in T cell-dependent activation, *J. Exp. Med. 177*, 1209−1213.
5. Mazzei, G. J., Edgerton, M. D., Losberger, C., Lecoanet-Henchoz, S., Graber, P., Durandy, A., Gauchat, J. F., Bernard, A., Allet, B., and Bonnefoy, J. Y. (1995) Recombinant soluble trimeric CD40 ligand is biologically active, *J. Biol. Chem. 270*, 7025−7028.
6. Stout, R. D., and Suttles, J. (1996) The many roles of CD40 in cell-mediated inflammatory responses, *Immunol. Today 17*, 487−492.
7. Uckun, F. M., Gajl-Peczalska, K., Myers, D. E., Jaszcz, W., Haissig, S., and Ledbetter, J. A. (1990) Temporal association of CD40 antigen expression with discrete stages of human B-cell ontogeny and the efficacy of anti-CD40 immunotoxins against clonogenic B-lineage acute lymphoblastic leukemia as well as B-lineage non-Hodgkin's lymphoma cells, *Blood 76*, 2449−2456.
8. Townsend, K. P., Town, T., Mori, T., Lue, L. F., Shytle, D., Sanberg, P. R., Morgan, D., Fernandez, F., Flavell, R. A., and Tan, J. (2005) CD40 signaling regulates innate and adaptive activation of microglia in response to amyloid β-peptide, *Eur. J. Immunol.* **35**, 901−910.
9. Banchereau, J., Bazan, F., Blanchard, D., Briere, F., Galizzi, J. P., van Kooten, C., Liu, Y. J., Rousset, F., and Saeland, S. (1994) The CD40 antigen and its ligand, *Annu. Rev. Immunol. 12*, 881−922.
10. Cella, M., Scheidegger, D., Palmer-Lehmann, K., Lane, P., Lanzavecchia, A., and Alber, G. (1996) Ligation of CD40 on dendritic cells triggers production of high levels of interleukin-12 and enhances T cell stimulatory capacity: T-T help via APC activation, *J. Exp. Med. 184*, 747−752.
11. van Kooten, C., and Banchereau, J. (2000) CD40-CD40 ligand, *J. Leukocyte Biol. 67*, 2−17.
12. Schonbeck, U., Sukhova, G. K., Shimizu, K., Mach, F., and Libby, P. (2000) Inhibition of CD40 signaling limits evolution of established atherosclerosis in mice, *Proc. Natl. Acad. Sci. U.S.A. 97*, 7458−7463.
13. Phipps, R. P. (2000) Atherosclerosis: The emerging role of inflammation and the CD40-CD40 ligand system, *Proc. Natl. Acad. Sci. U.S.A. 97*, 6930−6932.
14. Hirano, A., Longo, D. L., Taub, D. D., Ferris, D. K., Young, L. S., Eliopoulos, A. G., Agathanggelou, A., Cullen, N., Macartney, J., Fanslow, W. C., and Murphy, W. J. (1999) Inhibition of human breast carcinoma growth by a soluble recombinant human CD40 ligand, *Blood 93*, 2999−3007.
15. O'Grady, J. T., Stewart, S., Lowrey, J., Howie, S. E., and Krajewski, A. S. (1994) CD40 expression in Hodgkin's disease, *Am. J. Pathol. 144*, 21−26.
16. Tong, A. W., Seamour, B., Chen, J., Su, D., Ordonez, G., Frase, L., Netto, G., and Stone, M. J. (2000) CD40 ligand-induced apoptosis is Fas-independent in human multiple myeloma cells, *Leuk. Lymphoma 36*, 543−558.
17. Tamada, K., and Chen, L. (2005) Renewed interest in cancer immunotherapy with the tumor necrosis factor superfamily molecules, *Cancer Immunol. Immunother.*, 1−8.
18. Funakoshi, S., Longo, D. L., Beckwith, M., Conley, D. K., Tsarfaty, G., Tsarfaty, I., Armitage, R. J., Fanslow, W. C., Spriggs, M. K., and Murphy, W. J. (1994) Inhibition of human B-cell lymphoma growth by CD40 stimulation, *Blood 83*, 2787−2794.
19. Sotomayor, E. M., Borrello, I., Tubb, E., Rattis, F. M., Bien, H., Lu, Z., Fein, S., Schoenberger, S., and Levitsky, H. I. (1999) Conversion of tumor-specific CD4+ T-cell tolerance to T-cell priming through in vivo ligation of CD40, *Nat. Med. 5*, 780−787.
20. Eliopoulos, A. G., and Young, L. S. (2004) The role of the CD40 pathway in the pathogenesis and treatment of cancer, *Curr. Opin. Pharmacol. 4*, 360−367.
21. Uno, T., Takeda, K., Kojima, Y., Yoshizawa, H., Akiba, H., Mittler, R. S., Gejyo, F., Okumura, K., Yagita, H., and Smyth, M. J. (2006) Eradication of established tumors in mice by a combination antibody-based therapy, *Nat. Med. 12*, 693−698.
22. Chaussabel, D., Jacobs, F., de Jonge, J., de Veerman, M., Carlier, Y., Thielemans, K., Goldman, M., and Vray, B. (1999) CD40 ligation prevents *Trypanosoma cruzi* infection through interleukin-12 upregulation, *Infect. Immun. 67*, 1929−1934.
23. Chamekh, M., Vercruysse, V., Habib, M., Lorent, M., Goldman, M., Allaoui, A., and Vray, B. (2005) Transfection of *Trypanosoma cruzi* with host CD40 ligand results in improved control of parasite infection, *Infect. Immun. 73*, 6552−6561.
24. Diehl, L., den Boer, A. T., Schoenberger, S. P., van der Voort, E. I., Schumacher, T. N., Melief, C. J., Offringa, R., and Toes, R. E. (1999) CD40 activation in vivo overcomes peptide-induced peripheral cytotoxic T-lymphocyte tolerance and augments anti-tumor vaccine efficacy, *Nat. Med. 5*, 774−779.

25. Karpusas, M., Hsu, Y. M., Wang, J. H., Thompson, J., Lederman, S., Chess, L., and Thomas, D. (1995) 2 Å crystal structure of an extracellular fragment of human CD40 ligand, *Structure 3*, 1031−1039.
26. Banner, D. W., D'Arcy, A., Janes, W., Gentz, R., Schoenfeld, H. J., Broger, C., Loetscher, H., and Lesslauer, W. (1993) Crystal structure of the soluble human 55 kd TNF receptor-human TNFβ complex: Implications for TNF receptor activation, *Cell 73*, 431−445.
27. Rothe, M., Wong, S. C., Henzel, W. J., and Goeddel, D. V. (1994) A novel family of putative signal transducers associated with the cytoplasmic domain of the 75 kDa tumor necrosis factor receptor, *Cell 78*, 681−692.
28. Ishida, T., Mizushima, S., Azuma, S., Kobayashi, N., Tojo, T., Suzuki, K., Aizawa, S., Watanabe, T., Mosialos, G., Kieff, E., Yamamoto, T., and Inoue, J. (1996) Identification of TRAF6, a novel tumor necrosis factor receptor-associated factor protein that mediates signaling from an amino-terminal domain of the CD40 cytoplasmic region, *J. Biol. Chem. 271*, 28745−28748.
29. Vidalain, P. O., Azocar, O., Servet-Delprat, C., Rabourdin-Combe, C., Gerlier, D., and Manie, S. (2000) CD40 signaling in human dendritic cells is initiated within membrane rafts, *EMBO J. 19*, 3304−3313.
30. Faris, M., Gaskin, F., Parsons, J. T., and Fu, S. M. (1994) CD40 signaling pathway: Anti-CD40 monoclonal antibody induces rapid dephosphorylation and phosphorylation of tyrosine-phosphorylated proteins including protein tyrosine kinase Lyn, Fyn, and Syk and the appearance of a 28-kD tyrosine phosphorylated protein, *J. Exp. Med. 179*, 1923−1931.
31. Szocinski, J. L., Khaled, A. R., Hixon, J., Halverson, D., Funakoshi, S., Fanslow, W. C., Boyd, A., Taub, D. D., Durum, S. K., Siegall, C. B., Longo, D. L., and Murphy, W. J. (2002) Activation-induced cell death of aggressive histology lymphomas by CD40 stimulation: Induction of bax, *Blood 100*, 217−223.
32. Fournel, S., Wieckowski, S., Sun, W., Trouche, N., Dumortier, H., Bianco, A., Chaloin, O., Habib, M., Peter, J. C., Schneider, P., Vray, B., Toes, R. E., Offringa, R., Melief, C. J., Hoebeke, J., and Guichard, G. (2005) C3-symmetric peptide scaffolds are functional mimetics of trimeric CD40L, *Nat. Chem. Biol. 1*, 377−382.
33. Bianco, A., Fournel, S., Wieckowski, S., Hoebeke, J., and Guichard, G. (2006) Solid-phase synthesis of CD40L mimetics, *Org. Biomol. Chem. 4*, 1461−1463.
34. Changeux, J. P., Devillers-Thiery, A., and Chemouilli, P. (1984) Acetylcholine receptor: an allosteric protein, *Science 225*, 1335−1345.
35. Changeux, J. P., and Edelstein, S. J. (1998) Allosteric receptors after 30 years, *Neuron 21*, 959−980.
36. Colquhoun, D. (2006) The quantitative analysis of drug-receptor interactions: A short history, *Trends Pharmacol. Sci. 27*, 149−157.
37. Lortat-Jacob, H., Chouin, E., Cusack, S., and van Raaij, M. J. (2001) Kinetic analysis of adenovirus fiber binding to its receptor reveals an avidity mechanism for trimeric receptor-ligand interactions, *J. Biol. Chem. 276*, 9009−9015.
38. Vives, R. R., Sadir, R., Imberty, A., Rencurosi, A., and Lortat-Jacob, H. (2002) A kinetics and modeling study of RANTES(9−68) binding to heparin reveals a mechanism of cooperative oligomerization, *Biochemistry 41*, 14779−14789.
39. Zamzami, N., Marchetti, P., Castedo, M., Zanin, C., Vayssiere, J. L., Petit, P. X., and Kroemer, G. (1995) Reduction in mitochondrial potential constitutes an early irreversible step of programmed lymphocyte death in vivo, *J. Exp. Med. 181*, 1661−1672.
40. Winzler, C., Rovere, P., Rescigno, M., Granucci, F., Penna, G., Adorini, L., Zimmermann, V. S., Davoust, J., and Ricciardi-Castagnoli, P. (1997) Maturation stages of mouse dendritic cells in growth factor-dependent long-term cultures, *J. Exp. Med. 185*, 317−328.
41. Singh, J., Garber, E., Van Vlijmen, H., Karpusas, M., Hsu, Y. M., Zheng, Z., Naismith, J. H., and Thomas, D. (1998) The role of polar interactions in the molecular recognition of CD40L with its receptor CD40, *Protein Sci. 7*, 1124−1135.
42. Rose, G. D., Gierasch, L. M., and Smith, J. A. (1985) Turns in peptides and proteins, *Adv. Protein Chem. 37*, 1−109.
43. Venkatraman, J., Shankaramma, S. C., and Balaram, P. (2001) Design of folded peptides, *Chem. Rev. 101*, 3131−3152.
44. Bossen, C., Ingold, K., Tardivel, A., Bodmer, J. L., Gaide, O., Hertig, S., Ambrose, C., Tschopp, J., and Schneider, P. (2006) Interactions of tumor necrosis factor (TNF) and TNF receptor family members in the mouse and human, *J. Biol. Chem. 281*, 13964−13971.
45. Winzler, C., Rovere, P., Rescigno, M., Granucci, F., Penna, G., Adorini, L., Zimmermann, V. S., Davoust, J., and Ricciardi-Castagnoli, P. (1997) Maturation stages of mouse dendritic cells in growth factor-dependent long-term cultures, *J. Exp. Med. 185*, 317−328.
46. Henkel, T., Machleidt, T., Alkalay, I., Kronke, M., Ben-Neriah, Y., and Baeuerle, P. A. (1993) Rapid proteolysis of IκB-α is necessary for activation of transcription factor NF-κB, *Nature 365*, 182−185.
47. Aicher, A., Shu, G. L., Magaletti, D., Mulvania, T., Pezzutto, A., Craxton, A., and Clark, E. A. (1999) Differential role for p38 mitogen-activated protein kinase in regulating CD40-induced gene expression in dendritic cells and B cells, *J. Immunol. 163*, 5786−5795.
48. Yanagawa, Y., and Onoe, K. (2006) Distinct regulation of CD40-mediated interleukin-6 and interleukin-12 productions via mitogen-activated protein kinase and nuclear factor κB-inducing kinase in mature dendritic cells, *Immunology 117*, 526−535.
49. Mackey, M. F., Wang, Z., Eichelberg, K., and Germain, R. N. (2003) Distinct contributions of different CD40 TRAF binding sites to CD154-induced dendritic cell maturation and IL-12 secretion, *Eur. J. Immunol. 33*, 779−789.
50. Legembre, P., Beneteau, M., Daburon, S., Moreau, J. F., and Taupin, J. L. (2003) Cutting edge: SDS-stable Fas microaggregates: An early event of Fas activation occurring with agonistic anti-Fas antibody but not with Fas ligand, *J. Immunol. 171*, 5659−5662.

BI602434A